Calibration of Rogowski coils at frequencies up to 10 kHz using digital sampling

Djokic, Branislav

Publisher's version / Version de l'éditeur:
https://doi.org/10.1109/TIM.2009.2038029
IEEE Transactions on Instrumentation and Measurement, 59, 5, pp. 1303-1308, 2010-04-05

Calibration of Rogowski Coils at Frequencies up to 10 kHz Using Digital Sampling

Branislav Djokić, *Senior Member, IEEE*

***Abstract*—A new system for calibration of Rogowski coils at frequencies up to 10 kHz, based on a reference current transformer, a reference ac shunt, and a digital sampling system, is described in the paper. The calibration system has been automated, and its performance has been evaluated. At the frequency of 10 kHz, the calibration system is capable of generating currents up to 100 A. At power frequencies, it is capable of generating currents up to 2000 A. The best uncertainties ($k = 2$) of the calibration system are estimated to be less than 500 μA/A for magnitude and 500 μrad for phase at 10 kHz and an order of magnitude better at power frequencies.**

***Index Terms*—Calibration, current transformer (CT), digital sampling, Rogowski coil (RC).**

I. Introduction

ROGOWSKI coils (RCs) have been in use for more than 100 years [1] for magnetic potential measurements and for various current-sensing applications: protective relaying, measurements of high currents, impulse currents, and transient currents [2] in electrical power industry, resistance welding in automotive industry [3], plasma physics [4], and elsewhere. Their development over time has included innovative designs, new materials, machining techniques [5], and 2- or 3-D printed circuit board structures [6], [7]. The introduction of electronic devices, error-reducing techniques, digitization of output signals, and communication capabilities have contributed to the development of Rogowski coil-based measurement systems [8], [9].

Rogowski coil applications often have demanding performance requirements such as long-term stability, immunity to external electromagnetic fields, mutual inductance change with primary current conductor position, temperature variations, and low susceptibility to noise in the presence of small-signal levels. An increased interest in Rogowski coils in the last several years has resulted in requests for calibrations of coils of more advanced designs and performances. There are relatively few papers that address calibration issues [10]. In general, calibration systems should have uncertainties of at least four and preferably ten times smaller than those of devices under test, which makes the calibrations of Rogowski coils challenging.

Manuscript received June 26, 2009; revised September 7, 2009. Current version published April 7, 2010. The Associate Editor coordinating the review process for this paper was Dr. Subhas Mukhopadhyay.

The author is with the Institute for National Measurement Standards, National Research Council of Canada, Ottawa, ON K1A 0R6, Canada (e-mail: Branislav.Djokic@nrc-cnrc.gc.ca).

Color versions of one or more of the figures in this paper are available online at http://ieeexplore.ieee.org.

Digital Object Identifier 10.1109/TIM.2009.2038029

A high-accuracy system for traceable calibrations of Rogowski coils at power frequencies and currents up to 60 kA using digital sampling is described in [11]. The digital sampling system (DSS) is based on implementation of two identical nonsynchronous multirate digital filters. Using nonsynchronous sampling has an advantage of eliminating the need for synchronization with the input signal, e.g., by means of a phase-locked loop. It allows operation in a power–frequency range and, unlike the processing based on fast Fourier transform (FFT)/discrete Fourier transform (DFT), is not affected by spectrum leakage. An important characteristic of the algorithm is its capability to discern small phase differences, on the order of a few microradians, even at signals derived from the power line having a fluctuating frequency [12], which is difficult to achieve with FFT/DFT.

The calibration of Rogowski coils at high frequencies and with low uncertainties is very challenging. A number of difficulties arise even in the frequency range of several kilohertz. A calibration of Rogowski coils in the audio frequency range, at small currents, is described in [13].

This paper describes a system for calibration of Rogowski coils at higher currents and frequencies up to 10 kHz, initially presented in [14]. It is based on a reference current transformer (CT), a reference ac shunt, and a digital sampling system (DSS).

II. Rogowski Coil Calibration

An ideal RC is characterized by the mutual inductance M between the coil and the primary, which is usually a single-turn winding,

$$e = -M\frac{di}{dt} \tag{1}$$

where i is the primary current, and e is the electromotive force induced in the coil and present at the nonloaded coil output. For the reconstruction of the current signal, the coil output voltage is integrated by analog [15] or digital means [16].

Under ideal sinusoidal conditions, the coil mutual inductance can be determined as

$$M = \frac{1}{\omega}\cdot\frac{V}{I} \tag{2}$$

where I is the primary rms current, V is the coil open-circuit output rms voltage, and ω is the angular frequency, $\omega = 2\pi f$, f being the current/voltage frequency. The phase angle between the coil primary current I and the secondary voltage V is $\pm\pi/2$ rad, depending on how the marked terminals of the primary and the secondary are defined. The coil

transimpedance $Z_T = V/I$ is often used as a coil parameter at a given frequency. Under nearly sinusoidal conditions, the primary current can be derived from the voltage measured at the coil output

$$I = K_V \cdot V \cdot \frac{f_0}{f} \tag{3}$$

where V is the rms value (fundamental) of the actual voltage at the coil output, f_0 is the rated frequency, f is the actual frequency, I is the rms value (fundamental) of the actual primary current, and K_V is the coil's rated transformation ratio $(1/Z_T)$ at the frequency f_0 and at the rated primary current. If the coil output voltage is integrated, the term f_0/f in (3) disappears, V represents the rms value (fundamental) of the actual voltage after integration, and K_V includes not only the coil but also the means used for performing integration.

Calibrations of Rogowski coils under nearly sinusoidal conditions assume measurements of the ratio and phase difference between the coil output voltage and the primary current, at a given frequency and with a given burden (impedance) at the coil output, to determine the ratio and phase errors ε and φ, respectively,

$$\varepsilon\,[\%] = \left(K_V \frac{V}{I}\frac{f_0}{f} - 1\right) \cdot 100 \quad \varphi\,[\text{rad}] = \varphi_V - \varphi_I \pm \frac{\pi}{2} \tag{4}$$

where φ_V is the phase angle of the voltage V, and φ_I is the phase angle of the current I, φ_V and φ_I having a common phase reference, e.g., the start of observation. For reasons of coil sensitivity equalization in the manufacturing process, temperature stabilization, frequency-response shaping (damping), or testing with the rated (usually resistive) burden, the coil may be loaded with a resistance R_B from a few kiloohms to 100 kΩ, or more. This may be a single resistor or a resistor network, e.g., a resistive divider. In this case, the effective (trimmed) mutual inductance should be stated with a specified burden.

Nearly ideal sinusoidal conditions are difficult to achieve, particularly when generating larger currents. With the coil output voltage being proportional to the time derivative of the primary current, each harmonic in the primary current spectrum appears in the coil output voltage spectrum multiplied by its angular frequency, i.e.,

$$V = M\sqrt{\sum_{i=1}^{N_h}(2\pi f_i I_i)^2} \tag{5}$$

where N_h represents the highest harmonic order.

In addition to its mutual inductance M, which, in accordance with (1), fully characterizes an ideal coil, a real coil is also characterized by the coil resistance R_C, the self-inductance L_S, and the capacitance C_S, which includes the coil stray capacitance, shielding capacitance, and output cable capacitance, as shown by the Rogowski coil equivalent circuit in Fig. 1. The coil-distributed turn-to-turn capacitance is not shown. It should be noted that R_C and R_B may appreciably differ at higher frequencies from their dc values.

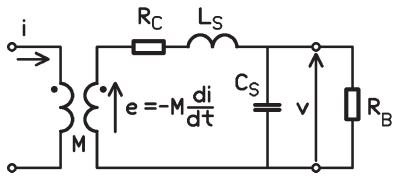

Fig. 1. Rogowski coil equivalent circuit with a burden.

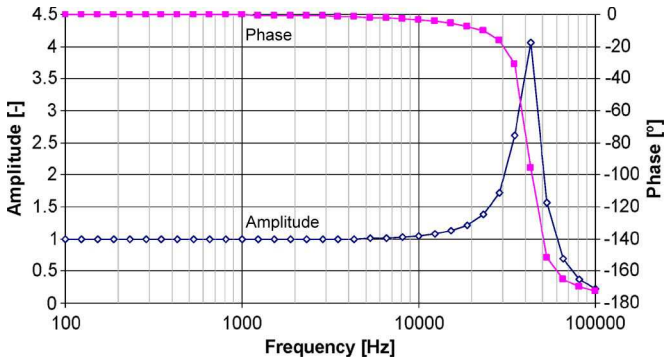

Fig. 2. Amplitude and phase-frequency characteristics of a Rogowski coil.

When setting up a calibration in a frequency range as opposed to a single frequency and at frequencies as high as 10 kHz, the amplitude and phase-frequency characteristics of the coil to be calibrated have to be taken into account. The amplitude characteristic represents a normalized coil output voltage versus frequency, at a constant primary current. How much this can matter is illustrated in Fig. 2 for a coil with values of $R_C = 100\ \Omega$, $L_S = 7$ mH, $C_S = 2$ nF, and $R_B = 10$ kΩ. This coil, which has a resonant frequency at 43.3 kHz and which in other respects may be perfect, at 10 kHz shows amplitude and phase deviations of 4.56% and $-3.39°$, respectively, from its ideal values. If a more accurate ac current measurement is wanted, either a coil with a sufficiently flat frequency response in the frequency range of interest has to be used, or the ac current value, obtained by measurement of the coil output voltage V, has to be corrected for these deviations according to the following equation:

$$I = j\frac{V}{M\omega}\left[1 + \frac{R_C}{R_B} - \omega^2 L_S C_S + j\omega\left(\frac{L_S}{R_B} + C_S R_C\right)\right] \tag{6}$$

where the expression in brackets represents the correction. The values of R_C, L_S, C_S, and R_B have to be established by separate measurements and calculations. The uncertainties in determining these values should be small enough so that the correction effectively reduces the coil errors. The calibration then determines the coil measurement uncertainties after this correction is applied.

For Rogowski coils, it is also important to test their sensitivity to the position of the primary current conductor inside the coil opening, to the positions of return conductors, to external electromagnetic fields, and to temperature changes. These tests are essential for determining the repeatability of the coil calibration results. Ideally, it should be known how, and under what conditions, the coil is going to be used so as to set the calibration according to those conditions and to ensure that the calibration results are meaningful and useful to the end user.

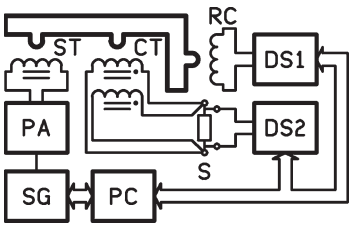

Fig. 3. Block diagram of the Rogowski coil calibration system.

If this is overlooked, the coil may operate in actual conditions with errors an order of magnitude, or more, larger than those obtained during the calibration.

III. Calibration System

Extending the calibration capability for Rogowski coils to higher frequencies is a demanding task both in terms of generating high currents and in terms of designing and calibrating pieces of the calibration equipment supposed to operate and retain their high performance at higher frequencies, including digital sampling system, and algorithms for determining the ratio and phase errors of the coils under test.

A simplified block diagram of the Rogowski coil calibration system is shown in Fig. 3. A signal generator SG drives a power amplifier PA, which, in turn, drives the primary of a current step-up transformer ST. The ST one-turn secondary generates current in the main current loop, as shown by the thick line. The main current loop passes as a single turn through the opening of a Rogowski coil. The coil output may be loaded with a specified burden according to the test requirements and is sampled by a digital sampler, DS1. A single-turn primary of a reference CT is part of the main current loop. The CT secondary provides the current for a reference ac shunt S used as a current-to-voltage converter. The shunt output voltage is the voltage replica of the main loop current and is sampled by another digital sampler, DS2. The SG and the digital samplers DS1 and DS2 are under control of a personal computer, PC.

A. Components

The high accuracy of the DSS in sampling directly low Rogowski coil output voltages was demonstrated in [11]; thus, using an ac shunt of special design [17] as an I/V converter with low output voltage was a viable option. This shunt allowed for operation at audio frequencies and provided low measurement uncertainties. Moreover, the shunt resistance of 0.1 Ω and the connection cable impedance represented a relatively small burden for the reference current transformer CT, thus keeping the reference CT measurement uncertainties low. The CT is a two-stage current transformer that has small, stable, and known errors under low-burden conditions.

B. Digital Sampling System

Digital sampling systems can implement various sampling techniques. In this application, a signal from an external source with accurate and stable time base is used as the sampling signal for simultaneous sampling of the primary current and the coil output voltage. Numeric integration of the output voltage

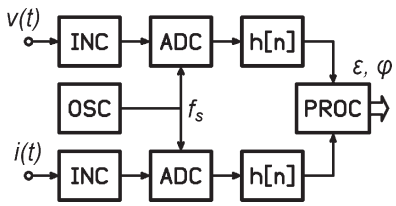

Fig. 4. Block diagram of the digital sampling system.

samples leads to reconstruction of the current. A calibration similar to those for current transformers can then be performed.

A possible approach to calibration under nearly sinusoidal conditions is to filter out the frequency components of interest from the measured, or sampled, signals representing replicas of the primary current and the coil output voltage. To extend the capabilities of the digital sampling to audio frequencies of up to 10 kHz, the use of bandpass digital filters was explored.

The block diagram of the DSS is shown in Fig. 4. INC represents the input signal conditioner, ADC represents the A/D converter of digital samplers, h[n] represents the bandpass digital filter, OSC is a source of the sampling frequency f_s, and PROC is a processing unit providing ratio and phase errors ε and φ, respectively, in accordance with (4).

The ratio and phase errors ε and φ, respectively, are calculated as

$$\varepsilon\,[\%] = \left(K_V \frac{f_0}{f} \sqrt{\frac{\sum_{k=1}^{n} v_k^2}{\sum_{k=1}^{n} i_k^2}} - 1 \right) \cdot 100 \tag{7}$$

$$\varphi = \arccos \frac{\sum_{k=1}^{n} v_k i_k}{\sqrt{\left(\sum_{k=1}^{n} v_k^2\right)\left(\sum_{k=1}^{n} i_k^2\right)}} \pm \frac{\pi}{2} \tag{8}$$

where v_k and i_k represent the *filtered* coil output voltage and primary current samples, respectively, including their proper scaling factors (originating from the CT transformation ratio, shunt resistance, A/D converter ranges, possible amplifier gains, resistive or inductive divider ratios, and other contributing factors present in the measurement chain), and n represents the number of samples in the measurement interval entailing as closely as possible an integer number of primary current periods. The rate of change of the cosine function is highest in the vicinity of $\pm\pi/2$ and so is the sensitivity of determining the phase error according to (8). At small primary currents, the uncertainties of ratio and phase errors determined by (7) and (8) increase.

C. Digital Samplers

The calibration applications require not only high resolution but also low uncertainties. To assure low uncertainties and the traceability of calibrations of Rogowski coils at operating frequencies up to 10 kHz, two commercially available sampling digital voltmeters (DVMs) are used. This achieves low-uncertainty performance of the DSS but constrains the maximum sampling rate to 50 kS/s for 18-bit resolution or 100 kS/s for 16-bit resolution.

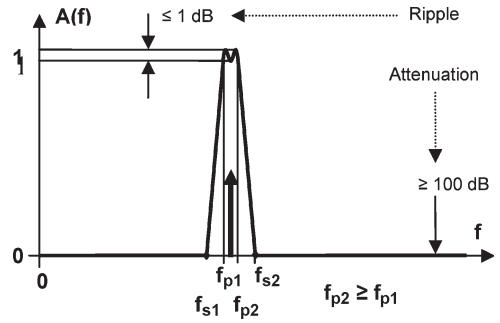

Fig. 5. Amplitude characteristic of the passband filter.

D. Digital Filter Design

The requirements for this application are different from those of nonsynchronous multirate digital filters described in [12]: 1) a bandpass filter (BPF) is needed instead of a low-pass filter (LPF); 2) BPF corner frequencies are not fixed as those of the LPF but have to follow the primary current frequency; and 3) the BPF amplitude ripple in the passband shown in Fig. 5 may be relaxed to 1 dB or more as opposed to the stringent ripple of $6.6 \cdot 10^{-5}$ dB of the aforementioned LPF. The applicability of the LPF filtering algorithm is bound to power frequencies.

In the present application, a large ripple in amplitude or a nonlinear phase of the filter characteristics do not affect, respectively, the ratio or the phase difference between the coil output voltage and the primary current, given by (7) and (8), respectively, at any operating frequency in the passband as long as both signals are filtered by identical filters.

Digital passband filters can be designed with a narrow passband such as 1 Hz. This narrow passband, however, extends the settling time of the filter output and increases the required data record length. The number of samples may be constrained by the available data memory of the digital sampler or, in the case of real-time processing, by the streaming data rate of the digitizer. Further consequence is a longer measurement/calibration time. A passband $f_{p2}-f_{p1}$ on the order of 10–50 Hz and an interval $f_{s2}-f_{s1}$ between the stopband corner frequencies of 100–500 Hz appear to be an acceptable tradeoff. With these specifications, elliptic and Chebyshev digital filters are designed for any central frequency in the range of interest. The attenuation in the passband filter stopbands was greater than 100 dB, as indicated in Fig. 5.

The passband filters are designed for predetermined frequencies of interest, their coefficients generated and saved in advance, or generated on the fly, and loaded during calibration based on the selected operating and sampling frequencies. If needed, the filter coefficients could be generated as the primary current frequency changes, which would represent an adaptive filtering application.

IV. Performance Evaluation

A. Current Generation Capability

The power amplifier used in this application operates at frequencies up to 11.5 kHz. Above this frequency, the amplitude of its output voltage starts dropping noticeably. The impact of the inductive load can be observed through the amplifier stability problems, which lead to oscillations at the operating frequencies and voltages much lower than those rated for both the amplifier and the current step-up transformer.

Two current step-up transformers of different designs were used as part of the calibration system. The step-up transformer with a higher current ratio has a higher number of turns, but it also has larger stray capacitances. Its secondary current at the rated primary voltage drops faster with the increase of frequency than that of the other step-up transformer under the same conditions.

The physical configuration of the main current loop in Fig. 3 is arranged to minimize its inductance and thus reduce, for the power amplifier, the current step-up transformer's reflected burden, which increases by square of the current transformation ratio. Since the burden that the loop inductance represents for the current step-up transformer and for the power amplifier directly increases with frequency, this appears as a significant constraint limiting the operating current to slightly above 100 A at 10 kHz using the current step-up transformer of the lower current ratio and higher bandwidth. Compensation of reactive power in the primary circuit of the current ST may ease the operating conditions of the power amplifier, but it does not mitigate the impact of the main current loop inductance on the required amplitude of the current step-up transformer primary voltage. Even if a power amplifier with a wider operating frequency bandwidth and a higher power rating is used, the voltage constraint of the current step-up transformer primary winding and its stray capacitances, which play a minor role at power frequencies, are limiting factors for producing high currents in the main loop at higher frequencies.

Since the distortion that the power amplifier may be introducing is of interest, the spectrum of the high-current signal generated by means of the power amplifier and the current step-up transformer was analyzed to assess requirements for the bandpass filter characteristics. No components of increased amplitude at frequencies up to 10 kHz were observed.

B. Voltage Calibration Capability

The sampling DVMs provide the best accuracy for peak voltages up to approximately 12 V. The operation at voltages up to 1000 V is readily available, but at increased measurement uncertainties. An alternative to that is scaling down the RC high-output voltage by other means, such as inductive or resistive voltage dividers. In that case, the divider uncertainties must be taken into account, as well as its input impedance loading the coil output, which may have to be increased by the design or by buffering. With an increase in voltage, the latter represents a challenge.

C. Simulation

The performance of the digital sampling algorithm and error calculations have been verified by simulations at various input current and sampling frequencies, various current and voltage levels, and various numbers of samples. In most cases, even at a low number of samples per period, the errors of calculated ratios and phase angles were below $50 \cdot 10^{-6}$ with respect to the

values set in simulation. As expected, more averaging helped in reducing the impact of noise added to current and voltage signals and the impact of the small number of samples at the higher end of the frequency range.

D. Component Calibrations

The performance of current transformers and current comparators at audio frequencies was explored in accordance with principles described in [18]–[20]. The in-phase and quadrature errors of the reference current transformer are estimated to be less than $20 \cdot 10^{-6}$ and $200 \cdot 10^{-6}$, respectively, at the actual burden of 0.2 Ω, at the ratios of 1 000 : 1 and 100 : 1, and the signal frequency of 10 kHz. These errors were repeatable and can be accounted for. The CT standard uncertainties were estimated to be less than $10 \cdot 10^{-6}$.

The ac shunt operated at currents not larger than 2 A, which is 20% of its rated current, and its self-heating was consequently 25 times smaller. The calibration of the ac shunt [21] has shown uncertainties $(k = 2)$ for both in-phase and quadrature components of less than $20 \cdot 10^{-6}$ in the frequency range up to 10 kHz.

To estimate the impact of the DSS input impedance on the measurement results, the input impedance was modeled as a simple parallel connection of a resistance and a capacitance. The measurements at various frequencies were performed with both samplers in their actual sampling mode during the measurement, using an additional resistor of known value. The input resistance value, which is on the order of hundreds of megaohms at low frequencies, drops down to approximately 1 MΩ at 10 kHz, whereas the input capacitance in the actual setup was measured to be about 275 pF and was changing within a few picofarads only in the same frequency range.

The uncertainty contribution by the stray capacitance of the two-twisted-pair cable between the reference CT secondaries and the shunt was explored by modeling the cable as a network of lumped resistances of the conductors and lumped capacitances corresponding to those among the conductors and the shield. Assuming a 3-m cable length, and representing the CT as a current source, the uncertainty was estimated to be below $1 \cdot 10^{-6}$ at 10 kHz.

The uncertainty of the shunt voltage due to the coaxial cable between the shunt and one of the digital samplers was less than $1 \cdot 10^{-6}$ at 10 kHz for the cable length of 1 m and was confirmed by both simulation and measurement using different coaxial cable lengths.

The impact of the DSS input impedance on the measured voltage at the Rogowski coil output depends on the Rogowski coil parameters, which include the coil output cable, and on the coil burden. Since the DSS input impedance is modeled as the parallel connection of the resistance R_D and the capacitance C_D, they are connected in parallel to the coil capacitance C_S and the burden R_B from Fig. 1. The correction shown earlier in (6) is thus modified into the new correction:

$$I = j\frac{V}{M\omega}\left\{1 + R_C\left(\frac{1}{R_B} + \frac{1}{R_D}\right) - \omega^2 L_S(C_S + C_D) + j\omega\left[L_S\left(\frac{1}{R_B} + \frac{1}{R_D}\right) + (C_S + C_D)R_C\right]\right\}. \quad (9)$$

TABLE I
UNCERTAINTIES OF THE CALIBRATION SYSTEM AT 10 kHz

Component	Ratio [10^{-6}]	Phase [10^{-6}]
CT 1,000:1	10	10
Shunt	10	10
Frequency	2	0
DSS	210	210
RSS (k=2)	421	421

The presence of the DSS input impedance effectively decreases the value of the burden R_B and increases the value of the capacitance C_S. For the values of the coil parameters and the burden given in the earlier example, these changes cause amplitude and phase deviations of 0.81% and $-0.16°$, respectively, at 10 kHz, from their values after the correction according to (6). The DSS input impedance is taken into account by applying the new correction (9) of the coil output voltage V in the measurement of the ac current I.

The DSS measurement uncertainty increases with frequency, and it is a challenge for evaluation at the input signal frequency of 10 kHz. Multiple DSS voltage ranges and various voltage ratios that have to be covered in a calibration further complicate the evaluation.

At a constant primary current, the coil output voltage increases with frequency according to (1). Since the maximum currents generated by the described calibration system decrease as the frequency increases, the maximum output voltage of the coil under calibration remains approximately constant at the maximum currents. The implication is that, at these maximum currents, the associated digital sampler operates at the same input voltage and voltage range, whereas the other digital sampler associated with the reference shunt operates at decreasing input voltages and lower voltage ranges as the frequency increases. The increasing voltage ratio with one of the voltages decreasing makes the evaluation of calibration uncertainties significantly more difficult. The operation of the digital samplers at different ranges also makes this evaluation more difficult.

Resistive and capacitive phase bridges [22] were used for calibrating phasewise a variable-frequency high-stability two-channel phase standard with resolution of 0.001° and independently adjustable amplitudes, which, in turn, was used for calibrating the DSS at frequencies up to 10 kHz. For ratio uncertainty evaluation, inductive voltage dividers and frequency-compensated resistive dividers with small output impedances are used, so that the DSS input impedance has an impact that may be neglected in the measurement.

The maximum value of the sampling rate limited to 50 or 100 kHz, depending on the selected resolution mode, results in a small number of samples of only five to ten per period of a 10-kHz input signal. Although the sampling rate is a limiting factor, the type-A standard uncertainty achieved by the DSS was smaller than $50 \cdot 10^{-6}$ at 10 kHz. The phase uncertainty verified by the aforementioned resistive and capacitive phase bridges is within ± 35 μrad. The type-B uncertainty of the DSS is estimated to be less than $200 \cdot 10^{-6}$ for both in-phase and quadrature components.

From the evaluated uncertainties of the main calibration system components, as shown in Table I, it is clear that the

DSS is the dominant factor in the calibration system uncertainty budget. Moreover, the DSS is the dominant factor in the whole frequency range up to 10 kHz, with the CT and ac shunt combined contribution to the root sum of squares of uncertainties being less than $2 \cdot 10^{-6}$ at the higher end of the frequency range. The overall calibration system uncertainty $(k = 2)$ at the signal frequency of 10 kHz is estimated to be within $500 \cdot 10^{-6}$ for both in-phase and quadrature components. To achieve this uncertainty, it was necessary to keep the DSS operating conditions under strict control, evaluate its performance at each frequency of interest, and put an effort into correcting all the parts of errors that are stable.

The aforementioned uncertainty is related to the described calibration system. It should be noted that the total uncertainty of the calibration depends in part on the type-A standard uncertainty of the Rogowski coil under test, which is usually much higher than the uncertainty of the calibration system.

V. Conclusion

A new system for calibration of Rogowski coil at frequencies up to 10 kHz, based on a reference current transformer, a reference ac shunt, and a digital sampling system, has been described. The calibration system is computer controlled, and its operation is automated. Magnitude and phase errors of the Rogowski coil under test are determined by digital sampling, with an optional numeric integration of the coil output signal. The calibration system performance has been evaluated. At the frequency of 10 kHz, the calibration system is capable of generating currents up to 100 A. At power frequencies, it is capable of generating currents up to 2000 A. The best uncertainties $(k = 2)$ of the calibration system are estimated to be less than 500 μA/A for magnitude and 500 μrad for phase at 10 kHz, and an order of magnitude less at power frequencies.

Acknowledgment

The author would like to thank the reviewers for their comments and R. Arseneau, D. Angelo, and D. Bennett of INMS/NRC, J. D. Ramboz of RAMTech Engineering, and D. E. Destefan of High Current Technologies for their useful suggestions.

References

[1] A. P. Chattock, "On a magnetic potentiometer," *Proc. Phys. Soc. London*, vol. 9, no. 1, pp. 23–26, Apr. 1887.
[2] D. A. Ward and J. L. T. Exon, "Using Rogowski coils for transient current measurements," *Eng. Sci. Educ. J.*, vol. 2, no. 3, pp. 105–113, Jun. 1993.
[3] D. E. Destefan and J. D. Ramboz, "Advancements in high current measurement and calibration," in *Proc. NCSLI Workshop Symp.*, 2000, p. 13.
[4] A. Werner, M. Endler, J. Geiger, and R. Koenig, "W7-X magnetic diagnostics: Rogowski coil performance for very long pulses," *Rev. Sci. Instrum.*, vol. 79, no. 10, pp. 10F 122/1–10F 122/4, Oct. 2008.
[5] J. D. Ramboz, "Machinable Rogowski coil, design, and calibration," *IEEE Trans. Instrum. Meas.*, vol. 45, no. 2, pp. 511–515, Apr. 2006.
[6] L. Kojovic, "PCB Rogowski coils benefit relay protection," *IEEE Comput. Appl. Power*, vol. 15, no. 3, pp. 50–53, Jul. 2002.
[7] N. Karrer and P. Hofer-Noser, "PCB Rogowski coils for high di/dt current measurement," in *Proc. IEEE PESC*, Galway, Ireland, Jun. 2000, pp. 1296–1301.
[8] D. Destefan, J. D. Ramboz, and S. Weiss, "Rogowski coil based systems to support utility and power industry current measurement needs," in *Proc. NCSL Int. Workshop Symp.*, Saint Paul, MN, 2007, p. 19.
[9] L. A. Kojovic, "Comparative performance characteristics of current transformers and Rogowski coils used for protective relaying purposes," in *Proc. IEEE PES General Meeting*, 2007, pp. 1–6.
[10] B. Djokic, "The design and calibration of Rogowski coils," *Measure, J. Meas. Sci.*, vol. 4, no. 2, pp. 62–75, Jun. 2009.
[11] B. Djokic, "Calibration of Rogowski coils at power frequencies using digital sampling," *IEEE Trans. Instrum. Meas.*, vol. 58, no. 4, pp. 751–755, Apr. 2009.
[12] B. Djokic and E. So, "Phase measurement of distorted periodic signals based on nonsynchronous digital filtering," *IEEE Trans. Instrum. Meas.*, vol. 50, no. 4, pp. 864–867, Aug. 2001.
[13] J. Bohaček and J. Kučera, "Calibration of Rogowski coils in audiofrequency range," in *Proc. 3rd Int. Conf. Metrology*, Tel Aviv, Israel, 2006.
[14] B. Djokic, "Calibration of Rogowski coils at frequencies up to 10 kHz using digital sampling," in *Proc. IEEE Conf. I2MTC*, Singapore, May 2009, pp. 437–441.
[15] C. D. M. Oates, A. J. Burnett, and C. James, "The design of high performance Rogowski coils," in *Proc. Int. Conf. Power Electron., Mach. Drives (Conf. Publ. No. 487)*, Jun. 2002, pp. 568–573.
[16] K. Schon and A. Schuppel, "Precision Rogowski coil used with numerical integration," in *Proc. 15th Int. Symp. High-Voltage Eng.*, Ljubljana, Slovenia, Aug. 2007.
[17] T. Tsuchiyama and T. Tadokoro, "Development of a high precision AC standard shunt for AC power measurement," in *Proc. IEEE CPEM*, Jun. 2002, pp. 254–255.
[18] N. L. Kusters and W. J. M. Moore, "The development and performance of current comparators for audio frequencies," *IEEE Trans. Instrum. Meas.*, vol. IM-14, no. 4, pp. 178–190, Dec. 1965.
[19] B. L. Dunfee and W. J. M. Moore, "An international comparison of current-ratio standards at audio frequencies," *IEEE Trans. Instrum. Meas.*, vol. IM-14, no. 4, pp. 172–177, Dec. 1965.
[20] W. J. M. Moore and H. Schlinke, "An international comparison of audio-frequency current transformer calibrations," *Metrologia*, vol. 8, no. 2, pp. 37–41, Apr. 1972.
[21] E. So, D. Angelo, T. Tsuchiyama, T. Tadokoro, B. C. Waltrip, and T. L. Nelson, "Intercomparison of calibration systems for AC shunts up to audio frequencies," *IEEE Trans. Instrum. Meas.*, vol. 54, no. 2, pp. 507–511, Apr. 2005.
[22] K. K. Clarke and D. T. Hess, "Phase measurement, traceability, and verification theory and practice," *IEEE Trans. Instrum. Meas.*, vol. 39, no. 1, pp. 52–55, Feb. 1990.

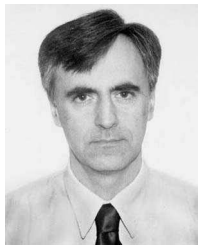

Branislav Djokić (M'90–SM'97) received the Dipl.Ing. degree in power systems engineering, the Dipl.Ing. degree in electronics, and the M.Sc. and Ph.D. degrees in electrical engineering from the University of Belgrade, Belgrade, Serbia, in 1981, 1984, 1988, and 1993, respectively.

From 1982 to 1990, he was with the R&D Institute Mihajlo Pupin, Belgrade, where he worked on development of industrial and high-accuracy systems for electrical power and energy measurements. From 1990 to 1994, he was a Staff Member of the School of Electrical Engineering, University of Belgrade. In 1994, he joined the Institute for National Measurement Standards, National Research Council of Canada, Ottawa, ON, Canada, where he has been working in the field of electrical power and energy measurements. His research interests entail high-accuracy measurement systems, data acquisition, measurement automation, and digital signal processing.

Dr. Djokić is a Registered Professional Engineer in the Province of Ontario. He is currently the Chair of the IEEE PES Emerging Technologies Coordinating Committee, past Chair of the IEEE Canada Other Societies Committee, and the Chair of the IEEE Ottawa Section Educational Activities.